PAPER

Simulating changes in shape of thermionic cathodes during operation of high-pressure arc discharges

IOP Publishing Journal of Physics D: Applied Physics

J. Phys. D: Appl. Phys. **52** (2019) 504004 (11pp) https://doi.org/10.1088/1361-6463/ab4510

Simulating changes in shape of thermionic cathodes during operation of high-pressure arc discharges

M D Cunha, H T C Kaufmann, D F N Santos and M S Benilov[1]

Departamento de Física, Faculdade de Ciências Exatas e da Engenharia, Universidade da Madeira, Largo do Município, 9000 Funchal, Portugal
Instituto de Plasmas e Fusão Nuclear, Instituto Superior Técnico, Universidade de Lisboa, 1049-001 Lisboa, Portugal

E-mail: benilov@uma.pt

Received 30 April 2019, revised 7 August 2019
Accepted for publication 16 September 2019
Published 9 October 2019

Abstract

A numerical model of current transfer to thermionic cathodes of high-pressure arc discharges is developed with account of deviations from local thermodynamic equilibrium occurring near the cathode surface, in particular, of the near-cathode space-charge sheath, melting of the cathode, and motion of the molten metal under the effect of the plasma pressure, the Lorentz force, gravity, and surface tension. Modelling results are reported for a tungsten cathode of an atmospheric-pressure argon arc and the computed changes in the shape of the cathode closely resemble those observed in the experiment. The modelling has shown that the time scale of change of the cathode shape during arc operation is very sensitive to the temperature attained by the cathode. The fact that the computed time scales conform to those observed in the experiment indicate that the model of non-equilibrium near-cathode layers in high-pressure arc discharges, employed in this work, predicts the cathode temperature for a given arc current with adequate accuracy. In contrast, modelling based on the assumption of local thermodynamic equilibrium in the whole arc plasma computation domain up to the cathode surface could hardly produce a similar agreement.

Keywords: thermionic cathodes, high-pressure arc discharges, deviations from local thermodynamic equilibrium, motion of the molten metal

(Some figures may appear in colour only in the online journal)

1. Introduction

Magnetohydrodynamic arc plasma simulations, coupled with simulations of melting of electrodes made of non-refractory metals (e.g. steel) and of motion of the melt, are state of the art in studies of gas metal arc welding (GMAW) and plasma cutting; e.g. reviews [1, 2]. A similar approach was applied recently to simulation of erosion of iron electrodes in a spark plug [3].

In contrast, numerical simulation of melting and motion of the melt of high-pressure arc electrodes made of refractory metals (e.g. tungsten) apparently has not been undertaken up to now. Such simulation is the subject of this work. The motivation is two-fold. First, it is the unrelieved use of arc technology with tungsten electrodes, tungsten inert gas (TIG) welding with low fume emission in particular.

The second aspect is methodological. All the above-mentioned arc plasma simulations, coupled with simulations of melting of electrodes and motion of the melt, rely on the assumption of local thermodynamic equilibrium, or LTE, in the whole arc plasma computation domain up to the electrode surfaces. Deviations from LTE occurring in the near-electrode regions, in particular, the near-cathode and near-anode space-charge sheaths, are not considered in the framework of this approach. On the other hand, significant effort has been invested by several groups around the world towards

[1] Author to whom any correspondence should be addressed.

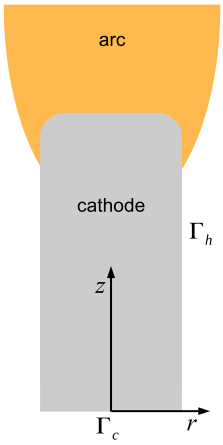

Figure 1. Geometry of the problem.

introduction of physically justified models of non-equilibrium near-electrode regions in high-pressure arc discharges; e.g. review [4] and references therein. It is very interesting to try to simulate current transfer from high-pressure arc plasmas to thermionic (refractory) cathodes, including motion of the molten metal and the change in shape of the cathode, with a physically justified account of deviations from LTE occurring in the near-cathode region, in particular, the near-cathode space-charge sheath.

A numerical model reported in this work aims to achieve this goal. The model is developed on the basis of the model of spots on non-thermionic (copper) cathodes of vacuum arcs [5] and of the model of initial phase of unipolar arcing on tungsten plates in fusion-related conditions [6]. The non-equilibrium near-cathode plasma layer is simulated by means of the model summarized in [7]. Computation results are reported for conditions of experiment with atmospheric-pressure argon arc with a tungsten cathode [8]. A good agreement between the modelling and the experiment is found. It appears that a similar agreement could hardly be achieved by means of LTE simulations.

The outline of the paper is as follows. The model is described in section 2. Numerical results on the changes in the cathode shape are given and discussed in section 3. Concluding remarks are given in section 4.

2. Numerical model

The cathodic part of a high-pressure arc discharge (the cathode and a thin near-cathode non-equilibrium layer) is governed primarily by processes in the non-equilibrium layer and, to a first approximation, is not affected by processes in the arc bulk. This allows one to decouple the calculation of the cathodic part of the arc from the calculation of the arc on the whole. This approach has been reasonably well established by now (e.g. discussion in [4]) and is used in this work.

The numerical model was developed on the basis of the models [5, 6] and is as follows. The system of equations comprises the time-dependent heat conduction equation, describing heat transfer in the cathode body with account of Joule heat production in the body of the cathode (including both the melt and the solid part); the equation of current continuity in the

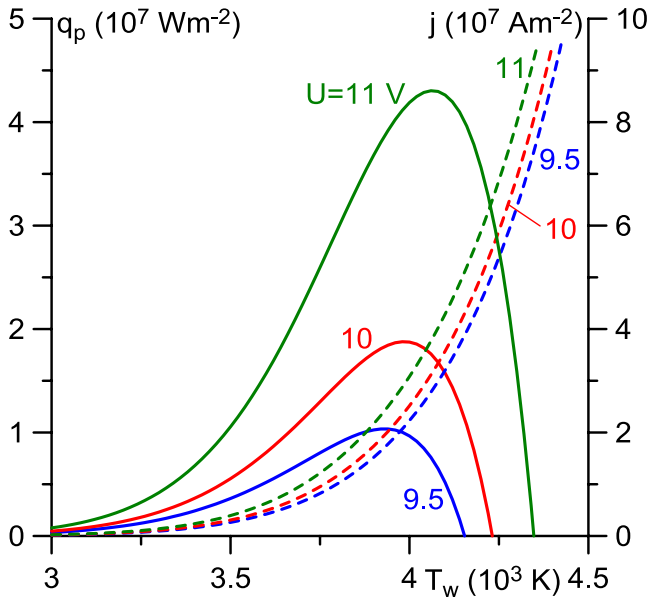

Figure 2. Densities of energy flux (q_p, solid) and electric current (j, dashed) to the cathode surface. Atmospheric-pressure argon plasma, tungsten cathode. T_w: local temperature of the cathode surface. U: near-cathode voltage drop.

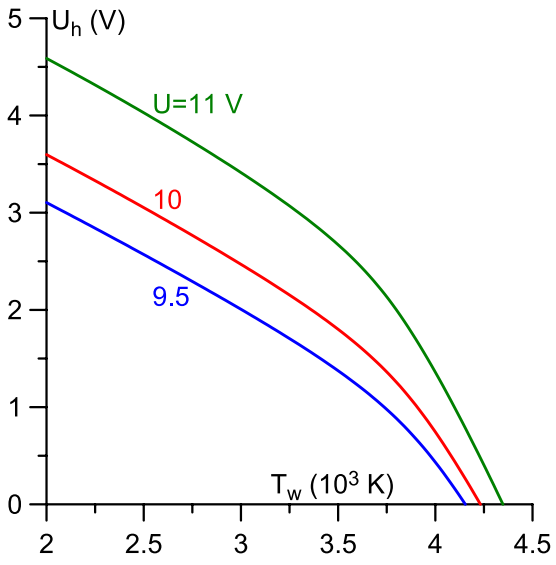

Figure 3. Cathode heating voltage $U_h = q_p/j$.

cathode body, supplemented with Ohm's law; and the continuity and Navier–Stokes equations, written for an incompressible fluid and describing the motion of the melt:

$$\rho c_p \frac{\partial T}{\partial t} + \rho c_p \mathbf{v}\cdot\nabla T = \nabla\cdot(\kappa\nabla T) + \sigma\left(\nabla\varphi\right)^2, \qquad (1)$$

$$\nabla\cdot\mathbf{j} = 0, \quad \mathbf{j} = -\sigma\nabla\varphi, \qquad (2)$$

$$\nabla\cdot\mathbf{v} = 0, \qquad (3)$$

$$\rho\frac{\partial\mathbf{v}}{\partial t} + \rho\left(\mathbf{v}\cdot\nabla\right)\mathbf{v} = \nabla\cdot\left[-p\mathbf{I} + \mu\left(\nabla\mathbf{v} + \left(\nabla\mathbf{v}\right)^T\right)\right] + \mathbf{j}\times\mathbf{B} + \rho\mathbf{g}. \qquad (4)$$

Here, ρ is the mass density of the cathode metal, c_p, κ, σ, and μ are, respectively, the specific heat, the thermal and

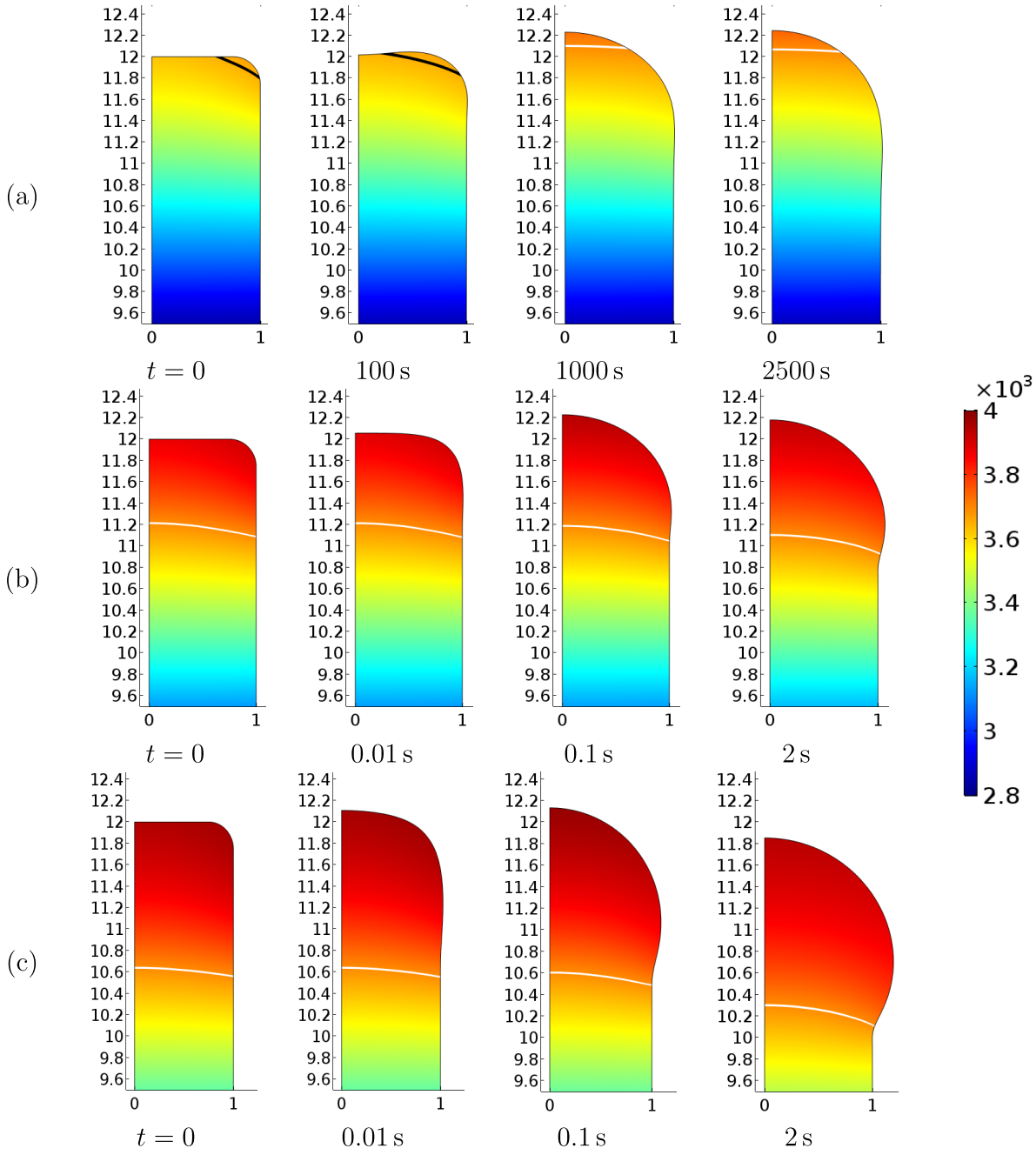

Figure 4. Evolution of the cathode shape. Distances in mm, temperature bar in K. (a) $I = 60$ A. (b) 140 A. (c) 200 A. White lines: isotherm of the melting temperature (3695 K). Black lines in the first and second images in figure (a) isotherm $T = 3650$ K.

electrical conductivities of the metal, and the viscosity of the melt (known functions of the temperature T), φ is the electric potential, $\mathbf{v}$ is the velocity, p is the pressure, $\mathbf{I}$ is the identity tensor, $\mathbf{j}$ is the density of electric current in the cathode body, $\mathbf{B}$ is the (self-induced) magnetic field, and $\mathbf{g}$ is the acceleration due to gravity. The second term on the left-hand side of equation (1) describes the convective heat transfer in the molten part of the cathode. The last two terms on the right-hand side of equation (4) represent, respectively, the Lorentz force and the gravity force.

The enthalpy-porosity method [9, 10] is used for modelling the solid–liquid phase transition in the metal, which implies solving equations (1)–(4) in the whole body of the cathode, including both the molten and solid parts (the solution for the velocity $\mathbf{v}$ vanishes inside the solid part). The account of the latent heat of melting is introduced along the same lines as is done in simulation of metal casting [11]. A front-tracking method is implemented for explicitly tracking the deformation of the molten surface on a moving grid.

The equations are solved under the assumption of axial symmetry in cylindrical coordinates (r, z); see figure 1. The magnetic field $\mathbf{B}$ only has the azimuthal component, which is related to the axial component of the current density in the cathode body by Ampère's law.

The base Γ_c of the cathode (figure 1) is maintained at a fixed temperature T_c by external cooling and the rest of the

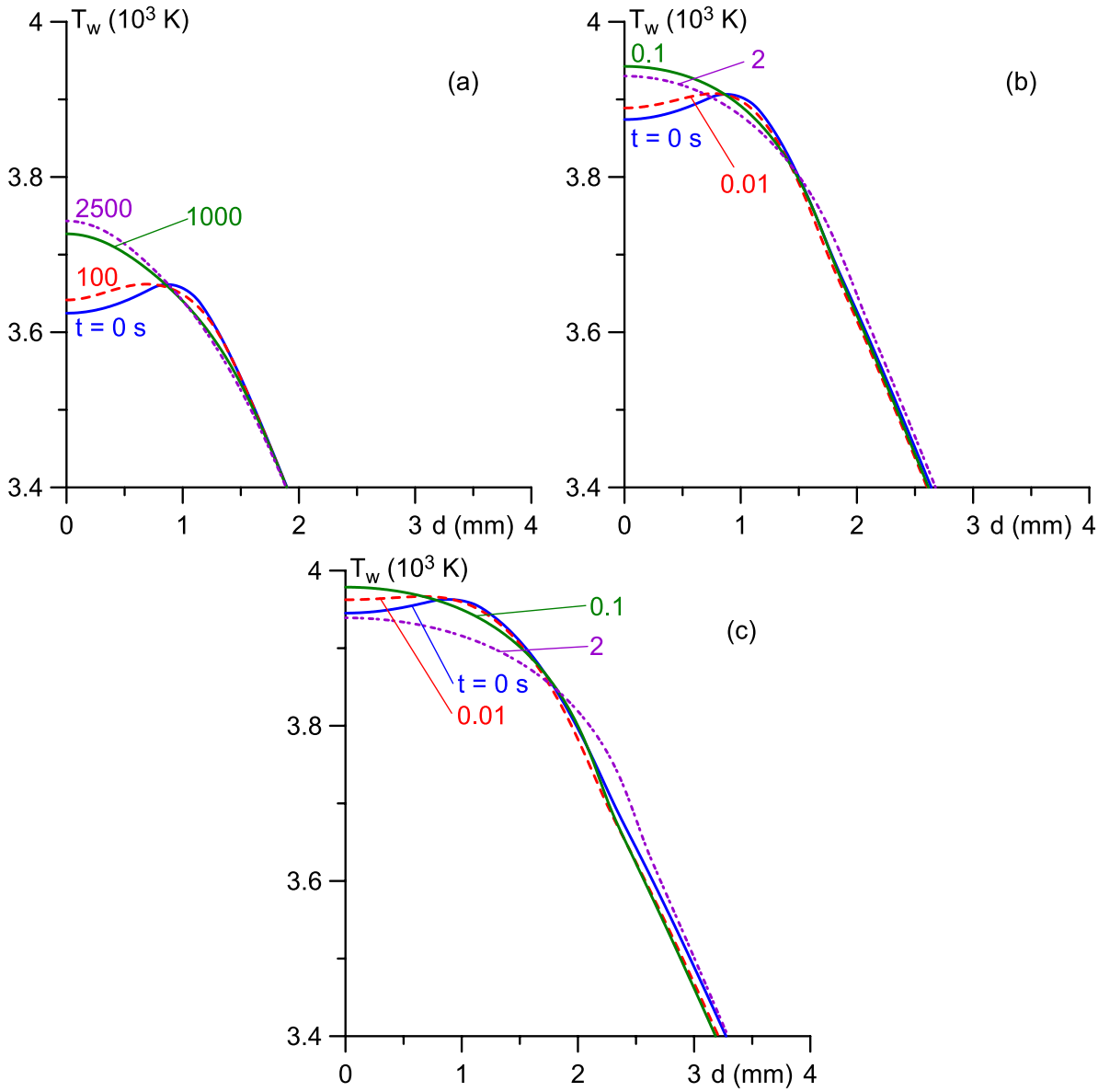

Figure 5. Distribution of temperature along the cathode surface. (a) $I = 60$ A. (b) 140 A. (c) 200 A.

cathode surface, Γ_h, is in contact with the plasma (or the cold gas) and exchanges energy with it and collects electric current. The boundary conditions for equations (1) and (2) are

$$\Gamma_c : T = T_c, \quad \varphi = 0; \qquad \Gamma_h : \kappa \frac{\partial T}{\partial n} = q, \quad \sigma \frac{\partial \varphi}{\partial n} = j. \quad (5)$$

Here, n is a direction locally orthogonal to the cathode surface and directed outside the cathode and q and j are densities of net energy flux and electric current coming from the plasma to the cathode surface. q is represented as $q = q_p - q_r$, where q_p is the density of net energy flux delivered to the cathode surface by the charged particles (the contribution of neutral atoms is neglected) and q_r is the density of losses of energy by the cathode surface through radiation. In the framework of the approach employing decoupling of the calculation of the cathodic part of the arc from the calculation of the arc on the whole (e.g. discussion in [4]), q_p and j are governed by properties of a thin near-cathode non-equilibrium layer and, while the temperature distribution in the cathode is being computed, may be treated as known functions of the local temperature T_w of the cathode surface and of the voltage drop U across the near-cathode layer: $q_p = q_p(T_w, U)$ and $j = j(T_w, U)$. U is assumed to be the same at all points of the arc attachment.

Forces due to the surface tension and the pressure exerted by the plasma on the cathode surface are introduced as boundary conditions for the Navier–Stokes equations at the cathode surface Γ_h. The force due to surface tension is evaluated in the usual way, in terms of the curvature of the molten metal surface and the surface tension of the cathode material. The pressure p_{pl} exerted over the cathode surface by the near-cathode plasma is estimated from the condition of equilibrium of the near-cathode layer:

$$p_{\mathrm{pl}} = p_{\mathrm{amb}} + \varepsilon_0 E_w^2/2, \quad (6)$$

where ε_0 is the permittivity of free space, p_{amb} represents the pressure exerted by the bulk plasma over the near-cathode layer (which equals the ambient pressure) and E_w is the electric field at the cathode surface. The second term on the rhs

describes the integral electrostatic force, applied by the electric field to the near-cathode layer per unit area.

Temporal variations of the thermal regime of the cathode and the motion of the melt develop on a time scale of fractions of seconds or slower. On the other hand, the biggest of time scales characterizing processes in the non-equilibrium near-cathode layer is the time of motion of the ions across the layer, which is typically of the order of 10^{-6} s or smaller. Therefore, in the investigation of the evolution of the temperature distribution and of the motion of the molten metal inside the cathode, processes on the plasma side can be considered as quasi-stationary. The only processes with inertia are heat propagation and motion of the molten metal in the cathode body; thus, nonstationary effects are accounted for only through the left-hand side terms in the heat conduction equation (1) and Navier–Stokes equation (4). This means, in particular, that the functions $q_p = q_p(T_w, U)$ and $j = j(T_w, U)$ can be calculated in the same way as in the steady-state case.

A model of non-equilibrium near-cathode layer in high-pressure arc discharges is needed in order to calculate these functions. Several such models are available in the literature; e.g. discussion in [12]. The model summarized in [7] is used in this work. Note that this model has gone through various validations by comparison with more sophisticated models and experimental data; e.g. reviews [4, 12]. A brief description of the model is given below for convenience.

The near-cathode layer is divided into a number of sublayers dominated by different physical mechanisms. The most important ones are a space-charge sheath, which is adjacent to the cathode surface, and an ionization layer, which is adjacent to the sheath. The model exploits the fact that a significant electric power is deposited by the arc power supply into the near-cathode space-charge sheath. A part of this power is transported by the ions and plasma electrons from the sheath to the cathode surface and heats the surface up to temperatures sufficient for thermionic electron emission. The rest of the deposited power is transported by the electric current into the arc column. Since the combined thicknesses of the space-charge sheath and the ionization layer are much smaller than a characteristic radius of the arc attachment, current transfer through the near-cathode layer is locally one-dimensional and all parameters of the layer, including q_p and j, are governed by the local surface temperature T_w and the near-cathode voltage drop U.

The ions going to the cathode and the electrons emitted from the cathode are accelerated in the space-charge sheath, which is considered as collisionless for ions; only simply charged ions are taken into account. The electron emission current from the cathode surface is evaluated by means of the Richardson–Schottky formula. The electric field at the surface, needed to determine the Schottky correction, is found by solving the Poisson equation in the sheath jointly with a kinetic equation describing the motion of the ions and the Boltzmann distribution for the plasma electrons (the space charge of the emitted electrons is neglected). The ion flux to the cathode is generated in the ionization layer. Equations of motion of the ion and atomic fluids in the ionization layer account for inertia, the pressure gradient, the electric field

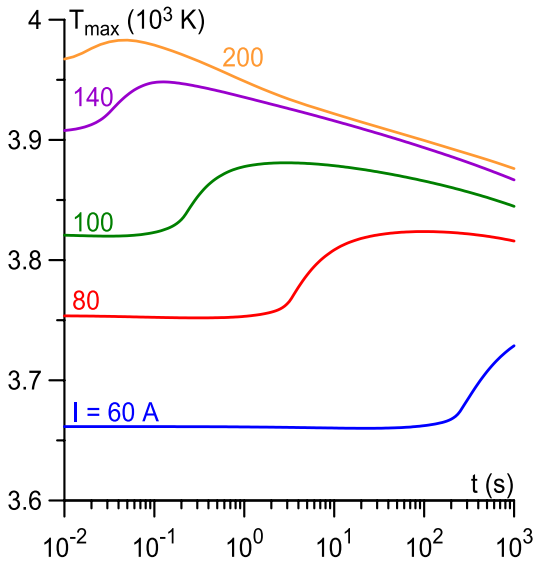

Figure 6. Evolution of the maximum temperature of the cathode.

force affecting the ions, momentum exchange (friction force) between the ions and the atoms due to elastic collisions, and momentum exchange due to volume ionization and recombination. The ionization equilibrium is assumed on the plasma side of the ionization layer, the Bohm criterion serves as a boundary condition on the sheath side. The equation of balance of the electron energy in the ionization layer is used in order to determine the electron temperature in the layer.

As an example, the densities of the energy flux and electric current from the atmospheric-pressure argon plasma to the surface of a tungsten cathode, given by this model, are shown in figure 2 for three values of the near-cathode voltage drop. The bell-shaped dependence of q_p on T_w, seen in this figure, is well known for both high-pressure and vacuum arcs (see [12] and references therein for high-pressure arcs and [13–15] for vacuum arcs) and represents the root reason of appearance of spots on arc cathodes. Without discussing this dependence in detail, we only note that the bell shape stems from a competition between the heating of the cathode surface by the ions coming from the plasma and the electron emission cooling. At relatively low T_w, the ionization degree of the plasma in the near-cathode layer increases with the increase in T_w and the ion heating increases faster than the emission cooling, so the net energy flux to the cathode surface increases. As T_w increases further and the ionization degree on the plasma side of the ionization layer approaches unity, the increase in the ion current slows down and the increase in electron emission cooling becomes dominant, so the net energy flux to the cathode surface starts decreasing. It is interesting to note that, while the variation of U by 1.5 V does not cause much change in values of the current density, the change in the energy flux density is appreciable.

It is of interest to evaluate, using the results shown in figure 2, the so-called cathode heating voltage, or volt equivalent of the heat flux to the cathode, $U_h = q_p/j$. Results of such evaluation are shown in figure 3. One can see that U_h is substantially smaller than the near-cathode voltage U, meaning that only a fraction of electrical energy deposited into the

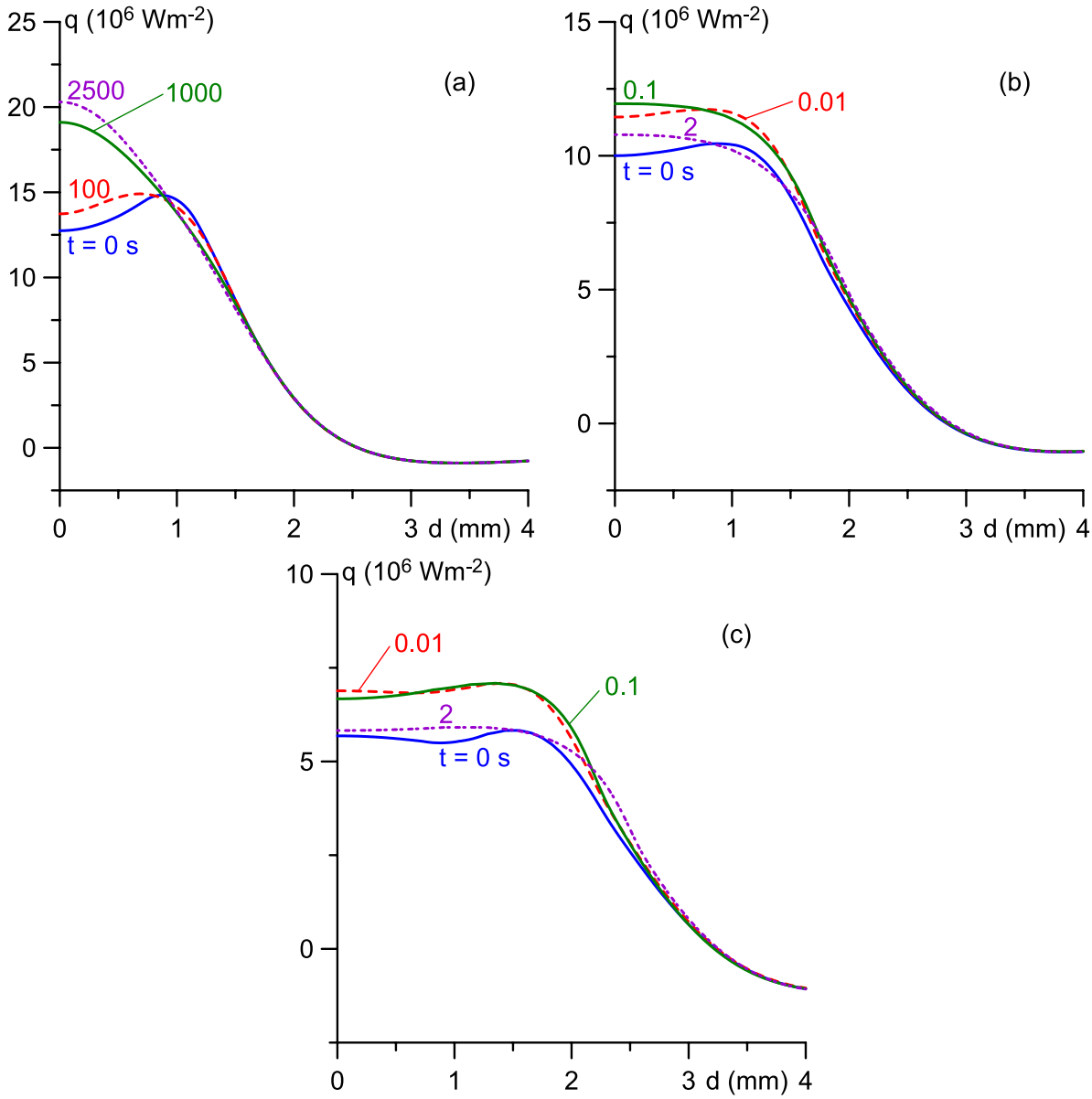

Figure 7. Distribution of the energy flux density along the cathode surface. (a) $I = 60$ A. (b) 140 A. (c) 200 A.

near-cathode layer is transported to the cathode, while the most part is transported by the electron current into the bulk plasma. The dependence of U_h on T_w and U is by no means weak, in other words, there is no proportionality between q_p and j in any meaningful sense. Hence, the concept of volt equivalent of the heat flux, while being useful for anodes of high-pressure arcs [16], is not applicable to cathodes.

3. Results and discussion

Numerical results given in this work refer to the simulation of the variation of shape of tungsten cathodes of atmospheric-pressure argon arc under conditions of the experiment [8]. In the experiments, fresh cathodes had the shape of a rod of 1 mm radius and 12 mm length; the working tip of the rod was flat with rounded edges (rounding radius 0.25 mm). Two forms of arc attachment to the cathode were observed, the diffuse mode and the spot mode; only the diffuse mode is simulated in this work. Since the cathode temperature is well below the boiling point of tungsten, the effect of tungsten vapor emitted by the cathode is not taken into account.

In the modelling, the temperature-dependent mass density, specific heat, thermal conductivity, viscosity, and surface tension are taken from [17]. The emissivity of tungsten, needed for evaluation of the losses of energy by the cathode surface through radiation, is taken from [18]. The value of 4.55 eV was assumed for the work function of pure (undoped) tungsten. The cooling temperature T_c was set equal to 300 K.

For each arc current value, the initial condition at $t = 0$ was obtained by computing steady-state current transfer for the same arc current with the hydrodynamics equations excluded. In other words, motion of liquid metal was not accounted for, so the cathode shape at $t = 0$ was that of fresh cathodes. The non-stationary modelling started at $t = 0$ with this initial condition and progressed until the cathode shape stopped changing.

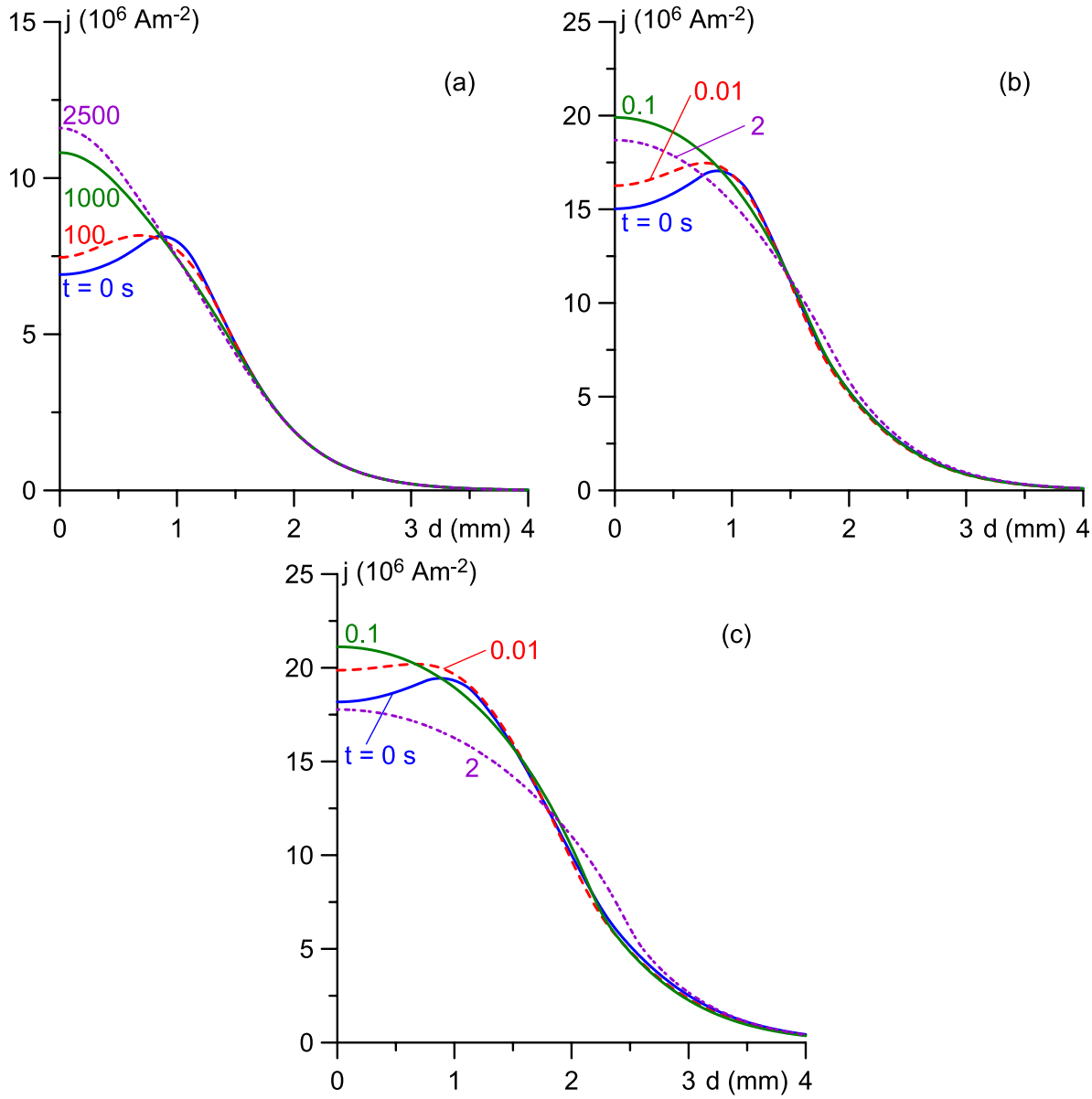

Figure 8. Distribution of the current density along the cathode surface. (a) $I = 60$ A. (b) 140 A. (c) 200 A.

The computed evolution of the cathode shape is shown in figure 4. Here and further only a part of the cathode near the tip is shown, distances are in mm, and white lines represent the isotherm of the melting temperature (3695 K). Note that for each current value the computed near-cathode voltage drop remained almost constant at all times in the modelling and equal to 10.9, 9.8, and 9.6 V for $I = 60$, 140, and 200 A, respectively. The shape of the cathode becomes more or less spherical in the end for all the three values of the arc current. For $I = 140$ and 200 A, the tip of the cathode becomes slightly compressed in the axial direction (i.e. acquires an oblate spheroidal shape) having a larger diameter than the diameter of the rod. The change of the cathode shape occurs on very different time scales: tens of minutes for $I = 60$ A and seconds for $I = 140$ and 200 A. These results are in a good agreement with the experimental observations [8]: if the arc attachment to a fresh cathode occurred in the diffuse mode, the shape of the cathode tip for $I \gtrsim 60$ A changed and became approximately hemispherical; this change took several tens of minutes for $I = 60$ A and occurred nearly instantly for $I = 140$–150 A; in the latter case, the tip of the cathode became slightly compressed in the axial direction having a larger diameter than the diameter of the rod [19].

The evolution of the surface temperature of the cathode is shown in figure 5. Here and further d is the distance from the center of the front surface of the cathode measured along the generatrix. At the beginning, when the cathode has a rod-like shape, the temperature takes the maximum value near the edge, where the conditions for heat removal by heat conduction are the worst. As the shape becomes more or less spherical, the maximum is shifted to the center. For $I = 60$ A, the maximum temperature is slightly lower than the melting temperature in the beginning and slightly higher in the end, which is why the melting isotherm is not seen in the first two

frames in figure 4(a) and is seen in the last two frames. The surface temperature increases with the increase in I and for $I = 200$ A approaches 4000 K.

The maximum of cathode temperature occurs on the surface in all the cases. The evolution of the maximum temperature for different currents is shown in figure 6. Clearly seen is the above-mentioned difference in time scales for different currents.

The evolution of the distributions of the net energy flux and electric current from the plasma to the cathode surface is shown in figures 7and 8, respectively. Both the energy flux density q in figure 7 and the current density j in figure 8 take maximum values at the same point that the surface temperature distribution in figure 5, which is a consequence of the near-cathode voltage U being assumed constant along the surface. Values of the current density in figure 8 increase with the increase in I as one could expect, which is due to the increase of the surface temperature T_w. In contrast, values of the energy flux density in figure 7 decrease with the increase in I; a somehow counter-intuitive effect caused by the reduction in the near-cathode voltage U, which overweighs the increase in T_w.

The evolution of the maximum speed of the melt for different arc currents is shown in figure 9. Let us consider the case $I = 140$ as a representative example. The melt velocity fields for three states marked by circles on the curve $I = 140$ A in figure 9 are shown in figure 10. The maximum speed $v_{\max}$ is of the order of 1 cm s^{-1} for t of the order of up to 10^{-2} s and decreases by about two orders of magnitude in the range of t of fractions of second, in which a circulation is formed (figure 9(b)). After that, $v_{\max}$ first slightly increases and then continues to decrease, albeit slowly; the circulation continues to exist (figure 9(c)).

Taking 2 N m^{-1} and 1 mm (the rod radius) as characteristic values of surface tension and melt pool dimension, respectively, one finds that the variation of pressure along the surface created by the surface tension is of the order of 2 kPa. The increase of pressure due to the electrostatic force, applied by the electric field to the near-cathode layer (i.e. the second term on the right-hand side of equation (6)), is up to 3 kPa. The pressure variation over the height of 1 mm due to gravity is 190 Pa. Characteristic values of the current density and self-induced magnetic field are 3×10^7 A m^{-2} and 20 mT, so the pressure difference created by the Lorentz force is of the order of 600 Pa. It follows that the effect of pressure due to the electrostatic force is comparable to the effect of surface tension and the effects of the Lorentz force and gravity are minor.

In order to illustrate this conclusion, the variation of the shape of the cathode for $I = 200$ A was simulated neglecting the pressure increase due to the electrostatic force (i.e. dropping the second term on the right-hand side of equation (6)); in other words, the pressure exerted by the plasma over the cathode surface was set equal to 1 bar. The results are shown in figure 11. One can see that the effect of the electrostatic force is visible, although not strong: the cathode tip in the last image in figure 11 is a little closer to being spherical, rather than oblate spheroidal as in figure 4(c). In other words, the pressure increase due to the electrostatic force, applied by the

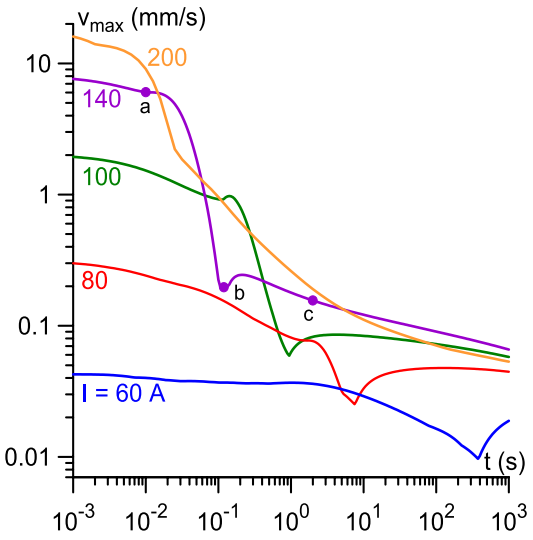

Figure 9. Evolution of the maximum speed of the melt. Points a, b, and c correspond to times $t = 0.01$, 0.12, and 2 s, respectively, and the corresponding velocity fields are shown in figure 10.

electric field to the near-cathode layer, causes a slight compression of the cathode tip in the axial direction; an understandable effect. One can even think of using experimental investigation of the deformation of thermionic arc cathodes at high currents for diagnostics of phenomena in the near-cathode layer.

The difference in the time scales of change of the cathode shape during arc operation for $I = 60$ and 140–200 A is a consequence of significantly different velocities of the molten metal: the maximum speed is of the order of 1 cm s^{-1} for 140–200 A and of the order of 40 μm s^{-1} for 60 A. These differences can be attributed to the temperature attained by the cathode: the maximum temperature is close to the melting temperature for $I = 60$ A and higher by some 250–300 K for $I = 140$–200 A. Note that the enthalpy-porosity method, which is used in this work for modelling the solid–liquid phase transition in the metal, may not be very accurate near the melting temperature, however it is correct qualitatively, therefore the above-discussed agreement with the experiment is not surprising. On the other hand, given the strong dependence of the time scale on the temperature attained by the cathode, which clearly is illustrated by figure 6, one should conclude that the model of non-equilibrium near-cathode layers in high-pressure arc discharges [7], employed in this work, predicts the cathode temperature for a given arc current with adequate accuracy.

As mentioned in the Introduction, numerical models based on the assumption of LTE in the whole arc plasma computation domain up to the electrode surfaces, coupled with simulations of melting of non-refractory electrodes and of motion of the melt, are state of the art in studies of GMAW and plasma cutting, however have apparently not been applied to electrodes made of refractory metals. One could ask what results LTE modelling would give for the conditions of the experiment with tungsten cathode [8], treated in this work. Of course, a detailed answer to this question is beyond the scope

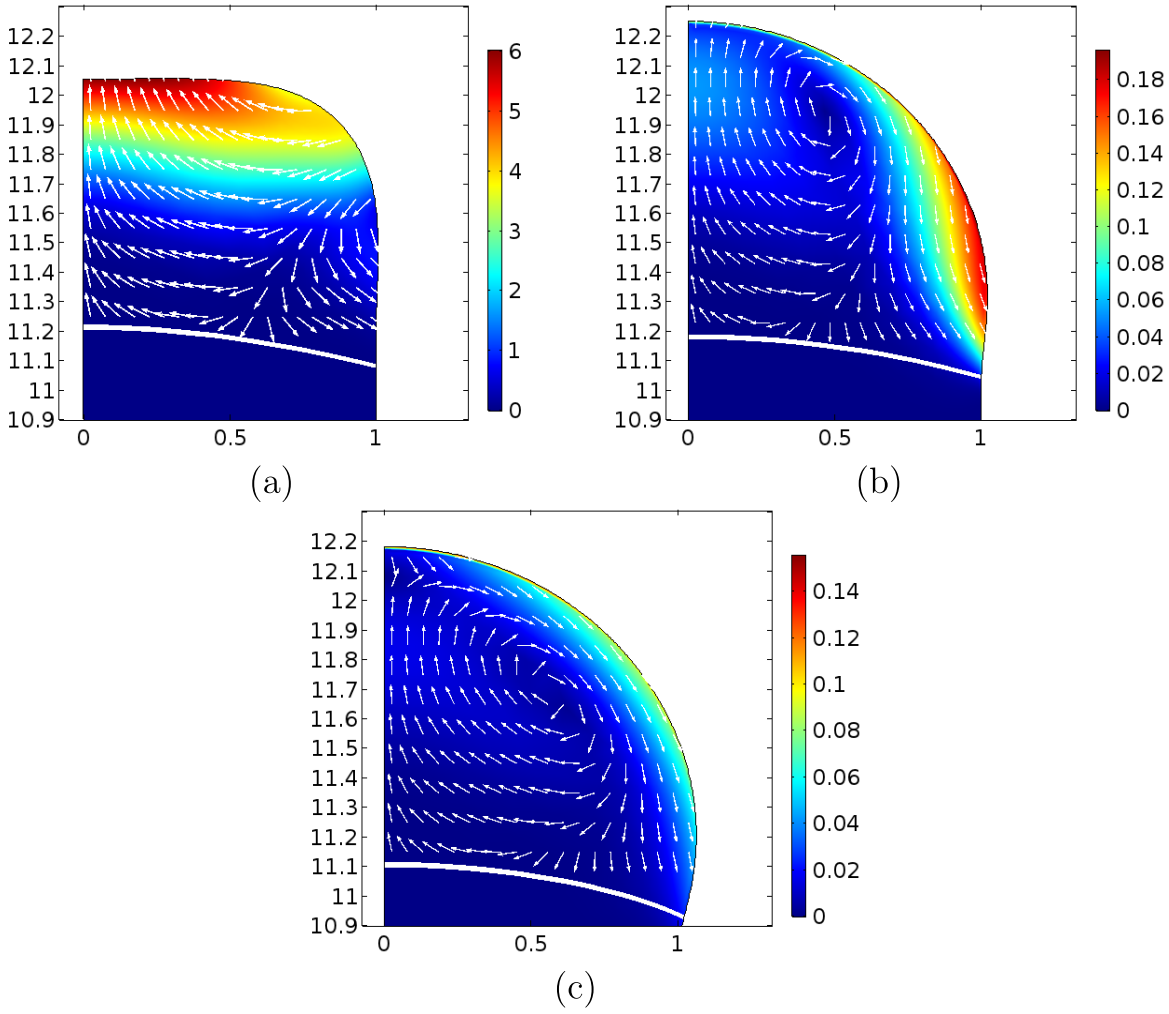

Figure 10. Evolution of the melt velocity field. Bars in mm s^{-1}. $I = 140$ A. (a) $t = 0.01$ s. (b) $t = 0.12$ s. (c) $t = 2$ s.

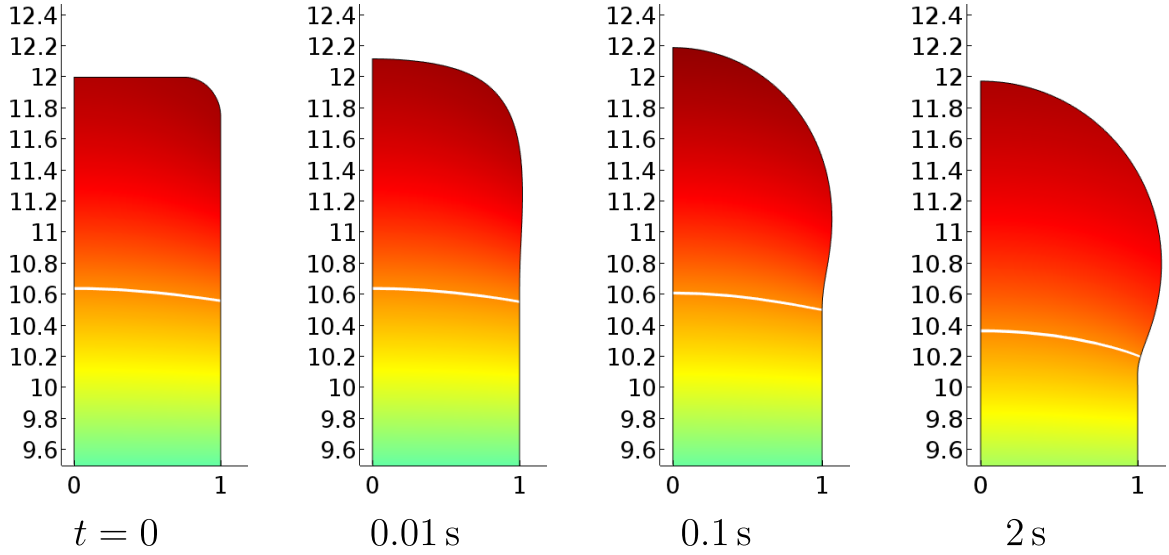

Figure 11. Evolution of the cathode shape computed neglecting electrostatic force. Temperature bar the same as in figure 4. $I = 200$ A.

of this work. However, some indications can be obtained from the LTE simulations for the conditions [8], which were performed in [20] in the steady-state approximation neglecting the motion of the melt and cathode shape variations.

First, it is worth recalling the comparison of arc voltages predicted by different models for the conditions [8] in the current range $I = 20$–175 A, reported in [21]. The LTE simulations [20] predicted a variation of the arc voltage with I that

was different from the experiment, while the non-equilibrium models agreed with each other and with the experiment reasonably well. In fact, this result was unsurprising. About two thirds of the arc voltage is contributed by the near-cathode sheath in these conditions. The LTE modelling neglects this contribution, on the one hand, and overestimates the resistance of the part of the arc column that is adjacent to the cathode, on the other. In the range of arc currents exceeding 120 A, the LTE modelling underestimates the experimental arc voltage by no more than approximately 2 V, which means that the two errors approximately compensate each other. However, it would be unrealistic to hope that such compensation will occur for all currents.

Second, the temperature at the center of the front surface of the cathode, evaluated in this work in the steady-state approximation neglecting the motion of the melt and cathode shape change, is given by values of T_w for $d = 0$ and $t = 0$ from figure 5: $T_w = 3625$, 3874, and 3945 K for $I = 60$, 140, and 200 A, respectively. The temperature at the center of the front surface of the cathode computed in the LTE simulations [20] was appreciably lower: 3268 and 3689 K for $I = 60$ and 160 A, respectively (values kindly provided by H-P Li). In light of the data shown in figure 6, these values suggest that in the framework of the LTE modelling the change of cathode shape for $I = 160$ A would occur significantly slower than in the experiment and there would be no change at all for $I = 60$ A.

In summary, existing data do not give reasons to hope that the LTE modelling of current transfer to thermionic (refractory) cathodes of high-pressure arc discharges could produce an agreement with the experiment similar to the one achieved by means of models taking into account deviations from LTE occurring near the cathodes.

4. Conclusions

A numerical model of current transfer to thermionic cathodes of high-pressure arc discharges is developed with account of deviations from local thermodynamic equilibrium occurring near the cathode surface, melting of the cathode, and motion of the molten metal under the effect of the plasma pressure, the Lorentz force, gravity, and surface tension. The model is applied to conditions of experiments with free-burning atmospheric-pressure argon arc with a rod tungsten cathode [8]. The modelling results reveal that in the case of the arc current of 60 A the shape of the cathode tip changed on the scale of several tens of minutes and became approximately hemispherical; the change occurred on the scale of seconds for current of 140 A and higher and the cathode tip became slightly compressed in the axial direction (i.e. acquired an oblate spheroidal shape) having a larger diameter than the diameter of the rod. This agrees well with the experimental observations [8].

The modelling has shown that the time scale of change of the cathode shape during arc operation is very sensitive to the temperature attained by the cathode: for the arc current $I = 60$ A, when the shape changed on the scale of tens of minutes, the maximum temperature of the cathode was close to the melting temperature of tungsten (3695 K); for $I = 140$ A, when the shape changed on the scale of seconds, the temperature was higher by some 250 K. The fact that these time scales conform to those observed in the experiment indicate that the model of non-equilibrium near-cathode layers in high-pressure arc discharges [7], employed in this work, predicts the cathode temperature for a given arc current with adequate accuracy. In contrast, the LTE simulations [20] predicted lower values of the cathode temperature, which would mean a shape change which occurs significantly slower than the one observed in the experiment, or no change at all. In other words, LTE modelling of current transfer to thermionic (refractory) cathodes of high-pressure arc discharges could hardly produce an agreement with the experiment similar to the one achieved by means of the model taking into account deviations from LTE occurring near the cathodes.

The above-mentioned slight compression of the cathode tip in the axial direction is owed, primarily, to the increase in pressure exerted by the near-cathode plasma over the cathode surface, which is due to the electrostatic force applied by the electric field to the near-cathode layer. In principle, one could think of using experimental investigation of the deformation of thermionic arc cathodes at high currents for diagnostics of phenomena in the near-cathode layer.

Results reported in this work are limited to the case where the arc attachment to the cathode occurred in the diffuse mode. Thus, interesting observations reported in [8, 22] for the case of the spot mode remain beyond the scope of this paper; an interesting possibility for future work.

Acknowledgments

The work was supported by FCT—Fundação para a Ciência e a Tecnologia of Portugal under Project UID/FIS/50010/2019 and by European Regional Development Fund through the Operational Program of the Autonomous Region of Madeira 2014–2020 under Project PlasMa-M1420-01-0145-FEDER-000016. The authors are grateful to Professor Sergey M Shkol'nik for discussion of the work [8] and to Professor He-Ping Li for supplying data on the cathode surface temperature from the LTE simulations [20].

ORCID iDs

M D Cunha https://orcid.org/0000-0002-0397-536X
H T C Kaufmann https://orcid.org/0000-0001-6740-2467
D F N Santos https://orcid.org/0000-0002-2377-766X
M S Benilov https://orcid.org/0000-0001-9059-1948

References

[1] Murphy A B, Tanaka M, Yamamoto K, Tashiro S, Sato T and Lowke J J 2009 *J. Phys. D: Appl. Phys.* **42** 194006
[2] Murphy A B 2015 *Plasma Chem. Plasma Process.* **35** 471
[3] Breden D P, Karpatne A and Raja L 2018 Modelling of electrode erosion for prediction of spark plug lifetime *SAE Technical Paper* 2018-01-0175 (https://doi.org/10.4271/2018-01-0175)

[4] Benilov M S 2019 *J. Phys. D: Appl. Phys.* accepted (https://doi.org/10.1088/1361-6463/ab47be)
[5] Kaufmann H T C, Cunha M D, Benilov M S, Hartmann W and Wenzel N 2017 *J. Appl. Phys.* **122** 163303
[6] Kaufmann H T C, Silva C and Benilov M S 2019 *Plasma Phys. Control. Fusion* **61** 095001
[7] Benilov M S, Cunha M D and Naidis G V 2005 *Plasma Sources Sci. Technol.* **14** 517
[8] Mitrofanov N K and Shkol'nik S M 2007 *Technol. Phys.* **52** 711
[9] Voller V R and Prakash C 1987 *Int. J. Heat Mass Transfer* **30** 1709
[10] Brent A D, Voller V R and Reid K J 1988 *Numer. Heat Transfer* **13** 297
[11] Lewis R W and Ravindran K 2000 *Int. J. Numer. Methods Eng.* **47** 29
[12] Benilov M S 2008 *J. Phys. D: Appl. Phys.* **41** 144001
[13] Shmelev D L, Delachaux T and Schade E 2013 *IEEE Trans. Plasma Sci.* **41** 384
[14] Almeida N A, Benilov M S, Benilova L G, Hartmann W and Wenzel N 2013 *IEEE Trans. Plasma Sci.* **41** 1938
[15] Shmelev D L, Barengolts S A and Tsventoukh M M 2017 *IEEE Trans. Plasma Sci.* **45** 3046
[16] Almeida N A, Cunha M D and Benilov M S 2017 *J. Phys. D: Appl. Phys.* **50** 385203
[17] Tolias P 2017 *Nucl. Mater. Energy* **13** 42
[18] Yih S W H and Wang C T 1979 *Tungsten: Sources, Metallurgy, Properties, and Applications* (New York: Plenum)
[19] Shkol'nik S M 2019 private communication
[20] Benilov M S, Benilova L G, Li H-P and Wu G-Q 2012 *J. Phys. D: Appl. Phys.* **45** 355201
[21] Lisnyak M, Cunha M D, Bauchire J-M and Benilov M S 2017 *J. Phys. D: Appl. Phys.* **50** 315203
[22] Hartmann T, Günther K, Lichtenberg S, Nandelstädt D, Dabringhausen L, Redwitz M and Mentel J 2002 *J. Phys. D: Appl. Phys.* **35** 1657